
Article:
Mangan, TP, Frankland, VL, Murray, BJ et al. (1 more author) (2017) The fate of meteoric metals in ice particles: Effects of sublimation and energetic particle bombardment. Journal of Atmospheric and Solar-Terrestrial Physics, 161. pp. 143-149. ISSN 1364-6826

https://doi.org/10.1016/j.jastp.2017.07.002

Accepted Manuscript

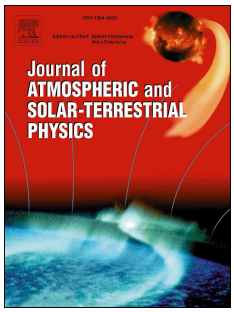

The fate of meteoric metals in ice particles: Effects of sublimation and energetic particle bombardment

T.P. Mangan, V.L. Frankland, B.J. Murray, J.M.C. Plane

PII: S1364-6826(17)30226-2

DOI: 10.1016/j.jastp.2017.07.002

Reference: ATP 4625

To appear in: *Journal of Atmospheric and Solar-Terrestrial Physics*

Received Date: 10 April 2017

Revised Date: 17 June 2017

Accepted Date: 6 July 2017

Please cite this article as: Mangan, T.P., Frankland, V.L., Murray, B.J., Plane, J.M.C., The fate of meteoric metals in ice particles: Effects of sublimation and energetic particle bombardment, *Journal of Atmospheric and Solar-Terrestrial Physics* (2017), doi: 10.1016/j.jastp.2017.07.002.

The fate of meteoric metals in ice particles: Effects of Sublimation and Energetic Particle Bombardment

T. P. Mangan[1], V. L. Frankland[1], B. J. Murray[2] and J. M. C. Plane[1]*

[1]School of Chemistry, University of Leeds, LS2 9JT.

[2] School of Earth and Environment, University of Leeds, LS2 9JT.

* corresponding author (email: j.m.c.plane@leeds.ac.uk)

Keywords:

Polar mesospheric clouds; Meteoric metals; Meteoric smoke particles; Energetic particle bombardment.

Abstract

The uptake and potential reactivity of metal atoms on water ice can be an important process in planetary atmospheres and on icy bodies in the interplanetary and interstellar medium. For instance, metal atom uptake affects the gas-phase chemistry of the Earth's mesosphere, and has been proposed to influence the agglomeration of matter into planets in protoplanetary disks. In this study the fate of Mg and K atoms, incorporated into water-ice films prepared under ultra-high vacuum conditions at temperatures of 110 to 140 K, was investigated. Temperature-programmed desorption experiments reveal that Mg- and K-containing species do not co-desorb when the ice sublimates, demonstrating that uptake on ice particles causes irreversible removal of the metals from the gas phase. This implies that uptake on ice particles in terrestrial polar mesospheric clouds accelerates the formation of large meteoric smoke particles (≥ 1 nm radius above 80 km) following sublimation of the ice. Energetic sputtering of metal-dosed ice layers by 500 eV Ar^+

and Kr^+ ions shows that whereas K reacts on (or within) the ice surface to form KOH, adsorbed Mg atoms are chemically inert. These experimental results are consistent with electronic structure calculations of the metals bound to an ice surface, where theoretical adsorption energies on ice are calculated to be -68 kJ mol^{-1} for K, -91 kJ mol^{-1} for Mg, and -306 kJ mol^{-1} for Fe. K can also insert into a surface H_2O to produce KOH and a dangling H atom, in a reaction that is slightly exothermic.

1. Introduction

In the terrestrial atmosphere, polar mesospheric clouds (PMCs) form in the summer high latitude mesopause region at altitudes between 82 and 88 km (Thomas, 1991). The clouds form at temperatures below 145 K and contain nanometre scale H_2O ice (Hervig et al., 2001). The ice particles typically sediment to the base of the ice layer (82 – 85 km) and grow to a median radius of 51 nm (von Cossart et al., 1999; Hervig et al., 2001), where the larger ice particles scatter sufficient sunlight to become optically visible. Mesospheric ice particles > 3 nm in radius are also responsible for radar echoes, known as polar mesosphere summer echoes (Rapp and Lubken, 2004).

In the PMC-forming region, metal layers formed via meteoric ablation are also present, peaking between altitudes of 85 to 93 km depending on the metal in question (Plane, 2003). Meteoric smoke particles (MSPs) formed from the condensation of ablated meteoric material are thought to act as nuclei for heterogeneous nucleation of the PMC ice particles (Saunders and Plane, 2006; Saunders et al., 2010; Hervig et al., 2012). As well as being involved in the initial nucleation of the ice particles, it has been shown that some metals can be efficiently removed from the gas phase in the vicinity of the clouds, because of efficient uptake on the ice surface (Murray and Plane, 2005). In the case of the Fe layer at the South Pole (which extends between 80 and 95 km with a peak around 87 km), substantial bite-outs in the layer were observed within strong PMCs (Plane et al., 2004). The significant removal of Fe and Na throughout the summer months at this location was attributed largely to removal on ice particles, although the temperature-dependence of the gas-phase chemistry also plays an important role (Gardner et al., 2005; Viehl

et al., 2015). Lidar measurements at Spitzbergen (78ºN) of the K layer (which peaks at 90 km and extends between 85 and 100 km), along with PMSE and PMC observations, showed a reduction in the underside of the layer in the presence of PMCs (Lübken and Höffner, 2004; Raizada et al., 2007). Satellite observations have also highlighted the correlation between PMC occurrence and depletion of the underside of the K layer at high latitudes (Dawkins et al., 2015). The Mg layer peaks at an altitude of 90 km and extends between 85 and 95 km (Langowski et al., 2015). Spaced-based measurements from the SCHIAMACHY spectrometer on the Envisat satellite showed an anti-correlation between Mg density and PMC radiance at high latitudes, which suggests that Mg may also be depleted by PMCs (Langowski et al., 2015).

Ice-metal interactions are also relevant to icy satellites, comets, asteroids, ice-covered dust particles in the interstellar medium (ISM), and the early stages of planet formation in protoplanetary discs (Pollack et al., 1994; Lewis, 2004; Campins et al., 2010; Filacchione et al., 2016; Driss et al., 2017). In the solar system, the terrestrial planets were formed primarily by the agglomeration of metal silicate and other metal-containing particles such as oxides and hydroxides. However, in the case of planetary formation in the outer solar system, the snow line (145 - 170 K) was where H_2O condensed into “dirty” ice particles on which metal uptake could occur (Podolak and Zucker, 2004). It has been proposed that these icy particles sufficiently enhanced the surface density available during accretion to form the gas giant planets of the outer solar system (Ciesla and Cuzzi, 2006; Pont, 2014). A model using Mg as a representative metal showed that accretion rates would have peaked at a radius in the protoplanetary disc where the Mg “freezes out” at temperatures between 150 K and 100 K (Dzyurkevich et al., 2013). The sublimation of dirty icy particles travelling

inward past the snow line may also have been important for introducing gas-phase species to the terrestrial planets (Cuzzi and Zahnle, 2004; Sato et al., 2016).

The uptake of Na, K and Fe atoms on low-temperature ice has been investigated experimentally. An uptake coefficient (γ) was measured for Na and K over the temperature range 80 - 150 K, with lower limits of γ_{Na} = > 0.05 and γ_{K} = > 0.09. The lower limits arise because when γ is large the loss of metal atoms becomes diffusion limited. In fact, electronic structure calculations show that Na and K bind strongly to ice, so γ is probably very close to unity (Murray and Plane, 2005). For Fe, γ_{Fe} also appears close to unity between 135 and 150 K, explaining the significant metal depletion observed in the vicinity of PMCs. More recently it was shown that Fe reacts on the ice surface to form $Fe(OH)_2$, and that it is sputtered efficiently from the ice surface by relatively low energy Ar^+ ions (< 500 eV) (Frankland and Plane, 2015).

Photoelectric emission from K, Na and Li deposited at low coverage on an ice surface has also been studied (Vondrak et al., 2006; Vondrak et al., 2009). The presence of these alkali metal atoms on the ice surface substantially reduces the photoelectric work function; however, the effect is short-lived (hundreds of seconds time scale at 92 K), presumably because the metals react in the ice to form hydroxides. Photoelectric emission of K doped ice layers (100 - 140 K) was also investigated by Yakshinskiy and Madey (2001) using X-ray photoelectron spectroscopy. They attributed a shoulder feature in the peak of the O 1s spectra as a reaction of K with the ice, suggesting KOH formation. However, there has not been a direct determination of the reaction products of K on ice.

Mg is the most abundant metal in chondritic meteorites, and the global injection flux of atomic Mg into the terrestrial atmosphere is predicted to be about 1.0 t d^{-1}, compared with 2.6 t d^{-1} of Fe (Carrillo-Sánchez et al., 2016). However, there do not

appear to have been previous experimental studies of the uptake and reactivity of Mg on ice. Here we report a laboratory study using an ultra-high vacuum (UHV) chamber to investigate the effects of thermal desorption and energetic ion sputtering of thin ice films on which Mg or K has been deposited, at temperatures between 110 – 140 K. Electronic structure calculations are then used to interpret the contrasting behaviour of these two metals. The role of uptake on ice particles as a route for effectively coagulating MSPs, metal atoms, and small metal-containing molecules (e.g. hydroxides) is then considered.

2. Experimental

2.1 Metal-Ice layer formation

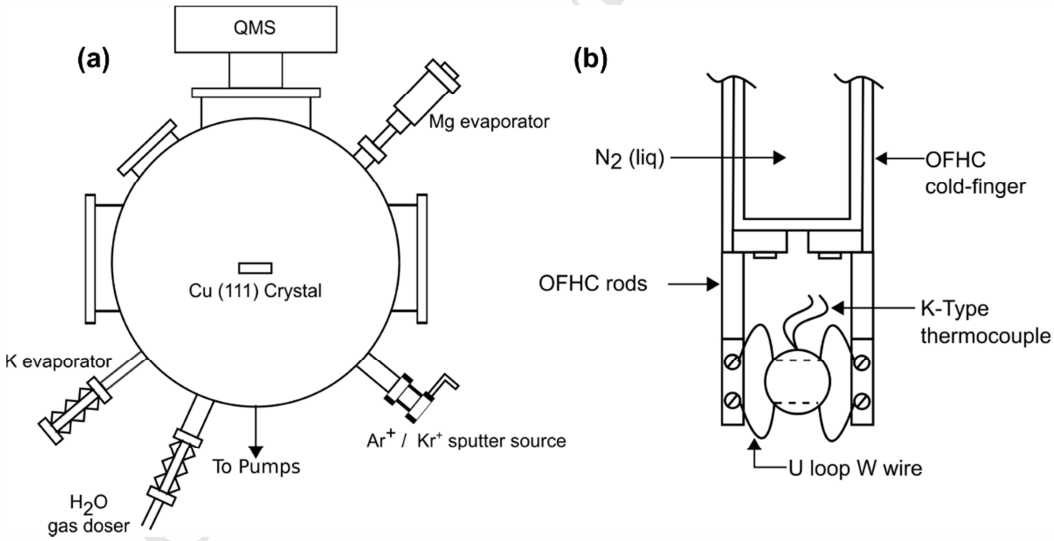

Figure 1. (a) Top down view of the UHV chamber; (b) front view of the Cu(111) sample mount.

Figure 1 is a schematic diagram of the UHV chamber and Cu(111) sample used in this study. This system has been described in part previously by Vondrak et al.

(2006) and is briefly described here with some modifications relevant to this study. The UHV chamber is a cylindrical stainless steel chamber with a diameter of 30 cm and a volume of approximately 25 L. This system is pumped down to pressures of 10^{-9} mbar by a 550 Ls^{-1} turbomolecular pump (Varian, TV551 Navigator), which in turn is backed by a high vacuum rotary pump (Varian, DS302). The chamber is equipped with a Quadrupole mass spectrometer (QMS) (Hiden, HAL 3F 301 RC PIC), a needle valve (NUPRO, SS4BK) for dosing H_2O and an inert ion (Ar^+ or Kr^+) sputter source (PSP Technology Ltd., ISIS3000). Mg was dosed using a Mg wire (Goodfellows, 99.9+ % purity) inserted into a monolayer deposition source (MDC vacuum, e-Vap 100), and K was dosed from a shrouded alkali metal dispenser (Saes Getters, K/NF/4.5/25 FT10+10).

Within the centre of the UHV chamber (Figure 1b) is a cylindrical Cu(111) crystal substrate, 12 mm in diameter and 2.5 mm thick, polished to 1 mm and oriented to 0.5° of the (111) plane. The Cu(111) crystal is mou nted via tungsten (W) heating wires onto an oxygen free high conductivity (OFHC) cold finger, which is controlled by an xyzθ manipulator. The substrate is liquid nitrogen cooled and heated resistively by the W wires embedded in the perimeter of the crystal. The temperature of deposited samples is monitored using a K-type thermocouple positioned in the side of the Cu(111) crystal. Prior to each experiment the Cu(111) crystal was cleaned by heating to 800 K for 30 min and when necessary sputtered by 500 eV Ar^+ or Kr^+ ions to remove any residual Mg or K.

In a typical experiment an H_2O ice film was deposited on the Cu(111) crystal using a purified source of H_2O, directed by the needle valve at the substrate (held at either 110 or 140 K) as an effusive collimated beam. To determine surface coverage, the pressure-dependent beam flux for H_2O was calibrated using the method described in

Mangan et al. (2015); for this study it was 5.5×10^{14} molecules cm^{-2} s^{-1}. For a 7200 s H_2O dose under the temperature conditions of this study (110 – 140 K), and using a H_2O sticking coefficient of 0.97 and ice density of 0.9 g cm^{-3} (Brown et al., 1996), a 1.3 µm thick ice film was deposited. At 110 K, amorphous ice was formed, while at 140 K a crystalline ice was formed. The crystal structure of the crystalline ice under these conditions may have been either a metastable stacking disordered state (with trigonal symmetry) or stable hexagonal ice (Malkin et al., 2015; Murray et al., 2015). An Mg or K layer was then dosed on top (surface) or in the middle (sandwich) of the ice film using the appropriate dosing apparatus. In the case of the sandwich experiments, a 0.65 µm ice film was first deposited on the Cu substrate, followed by the metal dose. Another 0.65 µm ice layer was then deposited on top of the metal. The metal layers deposited in these experiments were adsorbed for at least 60 minutes on the ice surface. This metal-ice layer was then subject to analysis via two different thin film techniques. The first was Temperature Programmed Desorption (TPD), which was used to investigate the thermal release from the ice layer of Mg- and K-containing species using a linear heating ramp of 0.5 ± 0.02 K s^{-1}. The second technique was energetic ion sputtering by 500 eV Ar^+ or Kr^+ ions directed at the sample. The energetic sputtering removes layers of the H_2O ice film and adsorbed metal species, effectively burrowing through the ice layer to provide a profile of the metal species present throughout the ice. The QMS was set at an electron impact ionization energy of 70 eV for all the results presented in this study, unless otherwise stated. The mass spectra shown of Mg-ice and K-ice sputtering were background corrected against a corresponding sputter profile of pure ice. These sputter profiles were also normalized in terms of fluctuations in the ion beam, measured as a change in the current to the sample via a pico-ammeter connected to the substrate.

3. Results

Before describing the results, it should be noted that the K and Mg metal dose rates could not be monitored during the dose, and were thus inferred by sputtering metallic species from the ice after the dosing was complete and any metal-ice processes had occurred. The dose rates were observed to be quite variable from day to day, presumably due to erosion of the metal targets inside the doser, so that up to an order-of-magnitude change in the total sputtered K or Mg signal could be observed between repeat experiments (where the cold stage temperature, water dose, sputter energy etc. are held constant). The experimental results presented here are therefore taken from the subset of experiments that did produce a comparable sputter signal for each metal, defined as the integrated sputter peak areas agreeing within 25%. Because of the variability in the metal dose between experiments it was not viable to explore aspects such as diffusion of the metallic species in the ice film. This issue does not affect the focus of the paper on residual formation after ice sublimation, and the reactivity of the metals within the ice.

3.1 Effect of ice sublimation on the adsorbed metals

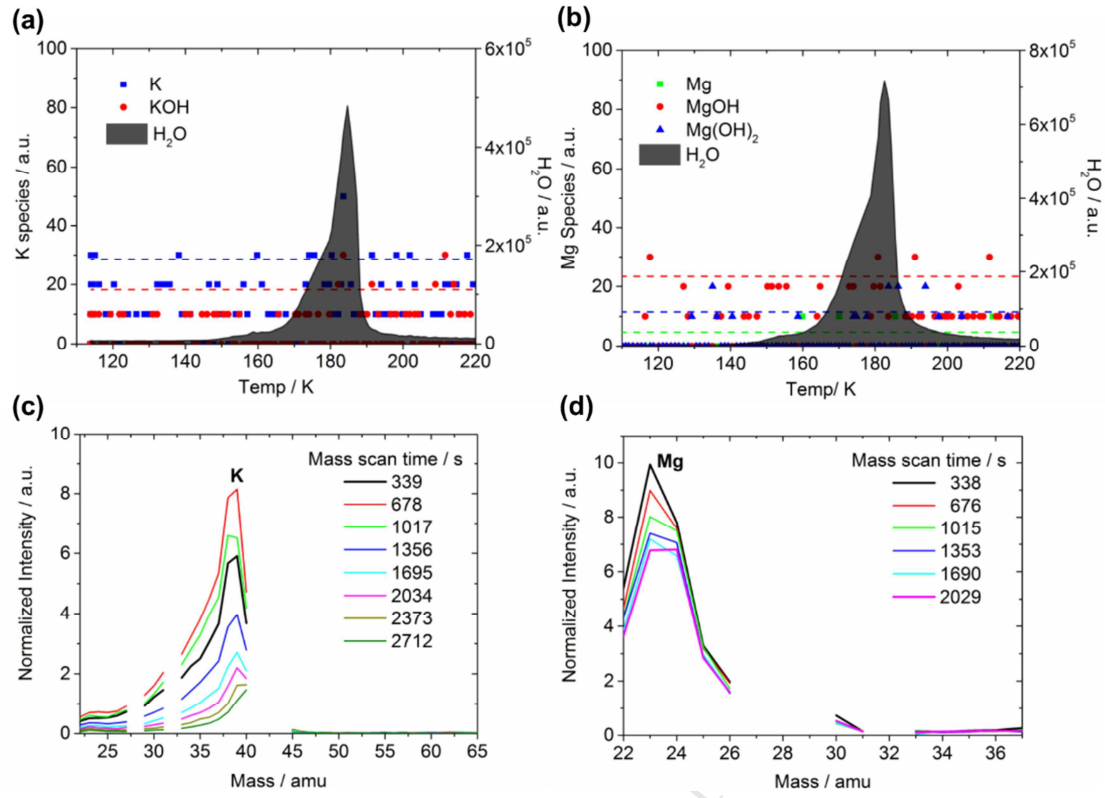

Figure 2: TPD traces of (a) K and (b) Mg that were dosed onto the surface of 1.3 µm layers of H_2O ice at 140 K are shown, including associated compounds. The dashed lines indicate the 3σ noise for the corresponding species. The lower panels show histogram mass spectra of (c) K at m/z = 39 and (d) Mg at m/z = 24 signals observed during energetic ion sputtering (by either 500 eV Ar^+ or Kr^+) of the Cu substrate after sublimation of the ice layer. m/z gaps in the sputter profiles correspond to the removal of background signals for N_2^+ (m/z = 28), O_2^+ (m/z = 32) and doubly-charged Kr^{2+} (m/z = 42). A peak shift towards higher m/z at the later times in (c) is due to the increasing influence of the leading edge of the Kr^{2+} ion peak at m/z =42.

Mg and K dosed onto ice were subject to TPD by linearly heating the metal-ice samples and monitoring the resulting release of species during ice sublimation using the QMS. TPD traces for ice at 140 K are shown in panels (a) and (b) of Figure 2

(the corresponding traces for ice at 110 K are almost identical and so not included here). TPD traces of the 1.3 μm H_2O films exhibit a profile that is consistent with previous studies (Fraser et al., 2001). In the case of H_2O at 140 K (subsequently cooled to 110 K just before TPD), a crystalline ice is formed (Sack and Baragiola, 1993; Safarik and Mullins, 2004). As the temperature of the sample was increased from 110 K, sublimation of the ice was detectable at approximately 140 K, peaking at 183 K. If the adsorbed Mg and K did desorb from the ice layer, co-desorption would have peaked at approximately the same temperature as the crystalline ice. Co-desorption has been previously observed for loosely-bound gaseous species such as CO_2 in H_2O ice (Galvez et al., 2008; Mangan et al., 2015). However, as can be seen in panels (a) and (b) of Figure 2, the TPD traces for K and Mg are primarily within the background noise (3σ) suggesting that desorption of the metals was negligible. We also monitored other K and Mg species (KOH, MgO, MgOH, $Mg(OH)_2$) during the TPD experiments, but these displayed no detectable co-desorption peaks. This lack of co-desorption was also observed in TPD traces of Mg and K dosed onto amorphous ice at 110 K.

Panels (c) and (d) of Figure 2 show mass spectra of energetic ion sputtering (500 eV Kr^+ for K, 500 eV Ar^+ for Mg) of the Cu substrate carried out after the TPD. In both the case of Mg (m/z = 24) and K (m/z = 39), clear broad peaks were detected corresponding to the respective metal species. This observation reveals that instead of co-desorbing with the ice, Mg and K species are instead left behind as a residual on the substrate after the ice layer has sublimated, a process that has been observed previously in the case of Fe (Frankland and Plane, 2015).

234 **3.2 Effect of ion-sputtering on the adsorbed metals**

235

236

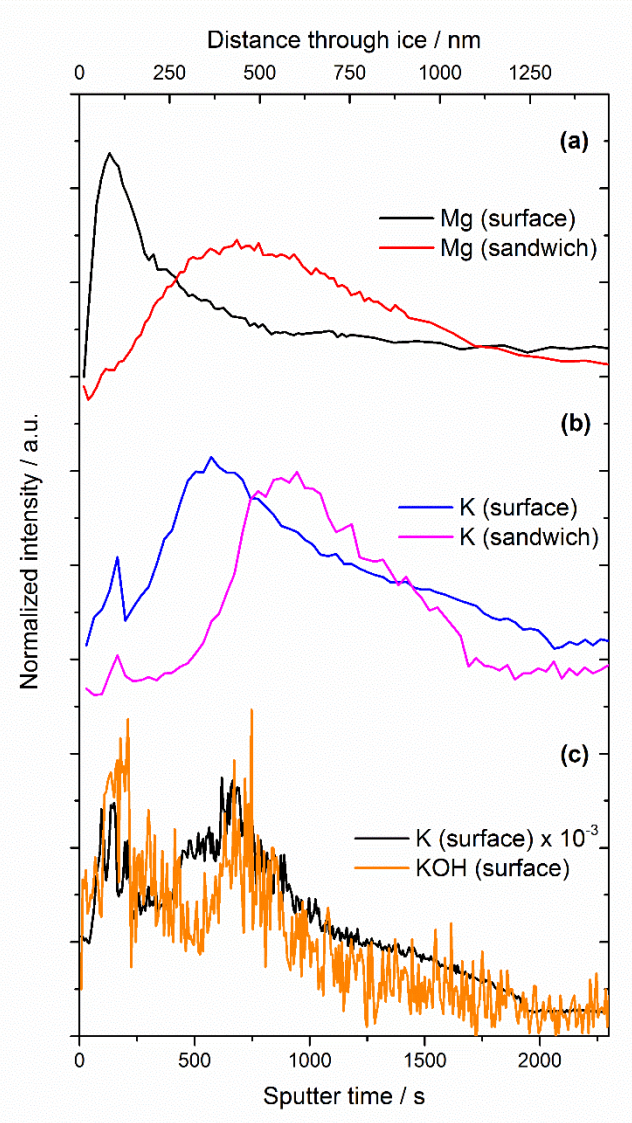

237

238 **Figure 3**. Vertically offset profiles of the normalized (a) Mg and (b) K signals
239 produced by energetic sputtering of metal-ice layers deposited at 110 K using
240 500 eV of Ar^+ or Kr^+ ions. The sputtering commenced 60 minutes are deposition was
241 complete. “Surface” profiles indicate metal adsorbed onto the 1.3 µm ice layer, while
242 “sandwich” profiles indicate when the metal was adsorbed between two 0.65 µm ice
243 layers. The QMS was set at an electron impact ionization energy of 70 eV for the

244 experiments shown in (a) and (b). (c) KOH is observed when the QMS was set to a
245 lower electron impact ionisation energy of 20 eV to reduce fragmentation of the KOH
246 product from the “surface” metal layer.

247 The normalized signals of gas-phase Mg and K species removed from H_2O ice via
248 energetic ion sputtering are shown in Figure 3. By monitoring the H_2O sputtering at
249 m/z=18 and knowing the H_2O ice thickness (1.3 μm), it was possible to convert the
250 sputter time (assuming a linear sputter rate) to an estimate of the distance through
251 the ice layer, shown on the top abscissa in Figure 3. It is clear from the profiles that
252 energetic sputtering by 500 eV Ar^+ and Kr^+ readily removes Mg and K from the ice
253 surface. The metal signals decrease to background levels by the time the energetic
254 sputtering has worked through the H_2O ice film and begun to sputter the Cu(111)
255 substrate below.

256 In the case of Mg (Figure 3a), the profiles of surface- compared to sandwich-
257 adsorbed Mg are quite different. The surface-adsorbed Mg exhibits a sharp peak ~80
258 nm below the surface of the ice layer. The roughly exponential decay in the signal
259 deeper into the ice film presumably results from diffusion of the Mg atoms through
260 the ice during the 60 minutes after deposition and before sputtering commenced.
261 The sandwiched H_2O-Mg-H_2O layer peaks closer to the middle of the ice layer
262 (~500 nm deep) as would be expected based on the deposition conditions, but is a
263 broader peak resulting from diffusion both towards the ice surface and the Cu(111)
264 substrate.

265 In the case of the profiles of K (Figure 3b), differences compared to the position of
266 the Mg within the ice layer are apparent: generally the K species migrate deeper in to
267 the ice, so that the surface-adsorbed K displays a broader primary peak that occurs
268 almost 300 nm deeper compared with the surface Mg. The peak K signal from the

sandwiched H_2O-K-H_2O layer is deeper into the ice than the respective Mg experiment, but shows a peak profile similar to the surface adsorbed K. A smaller secondary peak in the signal near the surface of the ice is observed at the same ice depth (~100 nm) in both K experiments. This comparable K ejection from different deposition conditions could be caused by K ejected during sputtering from a different surface such as the W mounting wires or Cu support arms where H_2O may also have been present. The reasons for these differences between the K and Mg peaks are unclear, and warrant investigation in the future with a better controlled metal doser that would permit time-resolved studies so that diffusion coefficients could be measured. Nevertheless, the results clearly demonstrate that both Mg and K are trapped in ice, are both reasonably mobile, and are released by energetic sputtering.

With the QMS set at an electron energy of 70 eV, no reactive products of Mg or K on the ice surface were detected. This could be due to a lack of reactivity between the metals with the ice, or because reaction products were fragmented within the QMS and not detected. To test if any reaction products were being fragmented at 70 eV, the electron impact ionization energy of the QMS was decreased to 20 eV. Once again, no reaction products for Mg were detected across a deposition temperature range of 110 – 140 K, suggesting Mg is unreactive when adsorbed on ice under these conditions. In contrast, for K adsorbed on ice (Figure 3c) a peak at m/z=56 was observed in the sputter signal, assigned as KOH. The corresponding K signal (also taken at an electron impact ionization energy of 20 eV) has been scaled to highlight the similar profile shape of K and KOH through the ice layer. Both the primary and secondary peaks of K and KOH occur at similar distances into the ice, suggesting KOH is formed wherever K is present. In the previous photoelectric emission study, the K signal on the ice decayed with an e-folding time of 200 s at 92

K (Vondrak et al., 2009). Given that the ice temperature in the present study was 110 K and the reaction rate is likely to have a positive temperature dependence by analogy with Na (Vondrak et al., 2006), and that there was a 60 minute delay between deposition of the K and sputtering in our experiments, it is very likely that complete conversion of K to KOH in the ice layer was occurring. The observed K signal at 20 eV would then be attributed to the majority of KOH formed on the ice still fragmenting under these conditions (an energy of 20 eV is the lower limit for stable operation of the QMS electron impact source). The differences between the K profiles at 70 eV (Figure 3b) and 20 eV (Figure 3c) are probably caused by the lack of reproducibility of the K atom doser, or possibly the different QMS settings employed to optimise the signal at each electron impact energy.

4. Electronic structure calculations

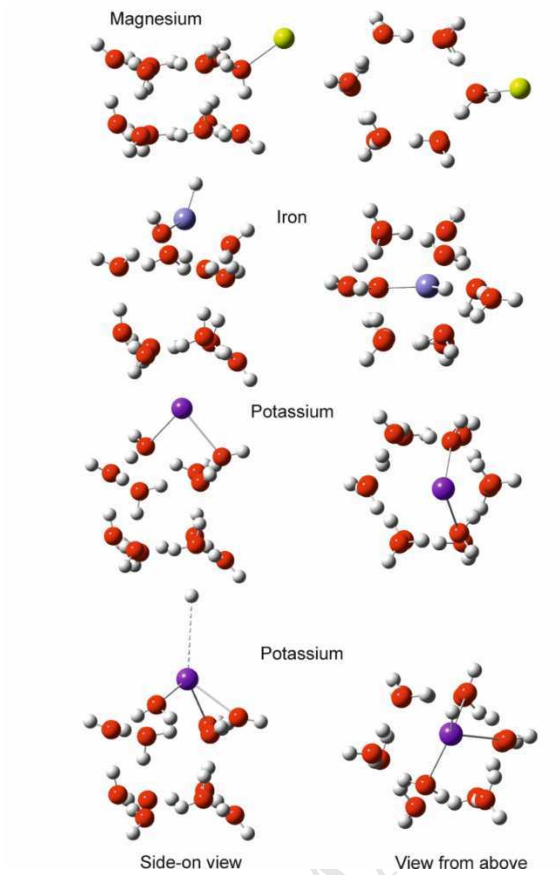

Figure 4. Structures of Mg, Fe or K bound to a model ice surface of 2 hexagonal rings of 6 H_2O molecules, calculated at the B3LYP/6-311+G level of electronic structure theory. Colour code: H, white; O, red; Mg, yellow; Fe, blue/grey; K, purple. The left-hand panels show the side-on view of the structures, and the structure viewed from above are shown in the right-hand panels. In the case of K, the additional panels at the bottom show the structure after the K atom inserts into a surface H_2O to form KOH and a dangling H atom. Without the metals present the 12 H_2O molecule system in Figure 4 would be observed as two perfectly mirrored hexagonal rings. Due to the strong binding of the metals to the ice (equivalent of 3+ hydrogen bonds), distortion of the H_2O rings occurs. Less distortion would be expected for a real ice surface, in which the H_2O rings are locked into sheets of hexagons.

To understand the experimentally observed reactivity of K and the inert nature of Mg bound to the ice surface as shown in Figure 3, electronic structure calculations of the metals binding to a model ice were undertaken. These were carried out at the B3LYP/6-311+G level of theory using the Gaussian 09 suite of programs (Frisch et al., 2009). We also include here calculations on Fe adsorbed on ice, in order to compare with our recent experimental study (Frankland and Plane, 2015). Figure 4 shows the optimized structures of Mg, Fe and K adsorbed on a model ice surface consisting of 12 H_2O molecules arranged in two stacked hexagonal rings. There are significant differences in the way the three metal atoms adsorb. In the case of Mg, the adsorption energy is -91 kJ mol^{-1}; however, the Mg is bound to the lone electron pair on a *single* H_2O molecule and is positioned on the outside of the hexagonal ring. Such a configuration would not be possible on a perfect sheet of hexagonal rings, but could occur on an imperfection such as a growth step or some other imperfection in the crystal structure. The Mg is therefore unreactive, consistent with the energetic particle bombardment results, but adsorbs relatively strongly at appropriate sites. This may explain the observation that surface deposited Mg remains closer to the ice surface than surface deposited K (see Figure 3a). Also, if the density of appropriate adsorption sites is low or the Mg cannot migrate across the surface to find such a site before desorbing again, it might be expected that the uptake coefficient of Mg on ice would be smaller than that of K and Fe.

The K adsorption energy is -68 kJ mol^{-1}. However, once adsorbed the K atom can insert into a surface H_2O, producing KOH embedded at the ice surface with a dangling H atom (bottom panels of Figure 4). This state is only 60 kJ mol^{-1} higher in energy than the initially adsorbed K atom. Thus, the overall process to form KOH is -8 kJ mol^{-1} i.e. slightly exothermic or perhaps thermoneutral, within the uncertainty at

this level of theory (Foresman and Frisch, 1996). In contrast, the *gas-phase* reaction $K + H_2O \rightarrow KOH + H$ is 171 kJ mol^{-1} endothermic (at the B3LYP/6-311+g(2d,p) level), illustrating the significant solvation of polar KOH on the ice surface. Once KOH has formed, the dangling H atom can easily migrate across the surface to find another dangling H and form H_2. The energy involved in converting the adsorbed K to KOH is consistent with the decay rate of K of 5×10^{-3} s^{-1} on ice at 92 K (Vondrak et al., 2009).

The Fe adsorption energy is -306 kJ mol^{-1}, because the Fe has inserted into a H_2O molecule to form the very stable HFeOH molecule bound to the surface. This is consistent with the observation of $Fe(OH)_2$ in the sputtering experiment of Frankland and Plane (2015). Note that in that earlier study we used electronic structure calculations to show that when Fe is bound to an H_2O trimer, there was a barrier of 70 kJ mol^{-1} for the Fe to insert into one of the H_2O molecules. Finding a free energy barrier to insertion into a H_2O molecule on the Fe-$(H_2O)_{12}$ system in the present study is computationally prohibitive. However, during the geometry optimization starting with a loosely adsorbed Fe, there was no indication of a barrier to insertion, probably because of additional stabilization from the H_2O ring structure. After the formation of HFeOH, further rearrangement with an adjacent H_2O on the surface should produce $Fe(OH)_2 + H_2$ without a significant activation barrier (see Figure 7 in Frankland and Plane (2015)).

5. Implications of metal uptake on PMCs - MSP coagulation

The present results show that Mg and K do not co-desorb with the ice layer during sublimation and instead the metals are left as residuals on the substrate surface. This has also been observed for Fe on ice (Frankland and Plane, 2015). The fact that these metals – whether atoms or compounds – do not sublimate but form a residual implies that the accumulation of meteoric compounds in PMC particles could leave relatively large residual particles when the ice sublimates, thus providing a distinct route to the formation of large MSPs in the vicinity of PMCs.

In the experiments in the present study, the 1.3 μm thick H_2O film was evaporated during the TPD runs in ~100 s, so that the film desorbed at a rate of ~13 nm s^{-1} (at a heating ramp of 0.5 ± 0.02 K s^{-1}). This rate is much faster than the maximum desorption rate of PMCs in the mesosphere, estimated by Gadsden (1982) to be about 0.6 nm s^{-1} (for a 50 nm radius ice particle at 170 K). It is unlikely that adsorbed metals on PMC particles undergoing this relatively slow evaporation rate would co-desorb, so that the conclusion from the present experiments should also hold for the sublimation of PMC particles. The sublimation of a metal-containing ice particle in the interplanetary or interstellar medium would typically be subject to even lower heating rates (≤ 0.1 nm s^{-1} for a 1 μm radius ice particle at ~170 K and 1 AU (Patashnick and Rupprecht, 1975)) compared to our experimental system, and so evaporation of the ice should also produce a metal-rich residual particle.

For PMCs this suggests that any metals removed from the gas phase onto the ice particle surface would be locked into the solid phase. As the region of the mesosphere warms, or the PMC particles sediment into a warmer and/or unsaturated region of the mesosphere, sublimation of the H_2O will commence. The metallic species will migrate deeper into the particle by diffusion until sublimation of the PMC particle is complete, leaving behind a residual particle composed of

394 adsorbed metal atoms, metal compounds, and MSPs, including the particle on which
395 the ice originally condensed. This process means that PMC particles in the Earth's
396 mesosphere will compete with MSP growth via coagulation and condensation of
397 metallic species from the gas phase, which in turn may influence the growth and
398 transport of MSPs during summer at high latitudes. Uptake of metals on PMCs is
399 therefore a distinct mechanism for creating MSPs, which could produce particles of
400 different morphology, density and composition compared to MSPs produced by
401 coagulation of existing “background” MSPs. Figure 5 is a comparison of the surface
402 area available for growth and coagulation on existing MSPs (taken from modelling
403 the distribution of charged particles measured by a rocket payload (Plane et al.,
404 2014)), compared with the surface area available on ice particles during a strong
405 PMC event (modelled from lidar backscatter measurements at South Pole (Plane et
406 al., 2004)). A strong PMC is classified as a cloud with a maximum backscatter
407 $\geq 1.3 \times 10^{-9}$ m^{-1} sr^{-1} at 532 nm (Fiedler et al., 2003), which corresponds to an ice
408 surface area of $\sim 5 \times 10^{-8}$ cm^2 cm^{-3} (Baumgarten et al., 2008). At the cloud peak, the
409 strong PMC provides at least 2 orders of magnitude greater available surface area
410 for metal uptake compared to the background MSPs.

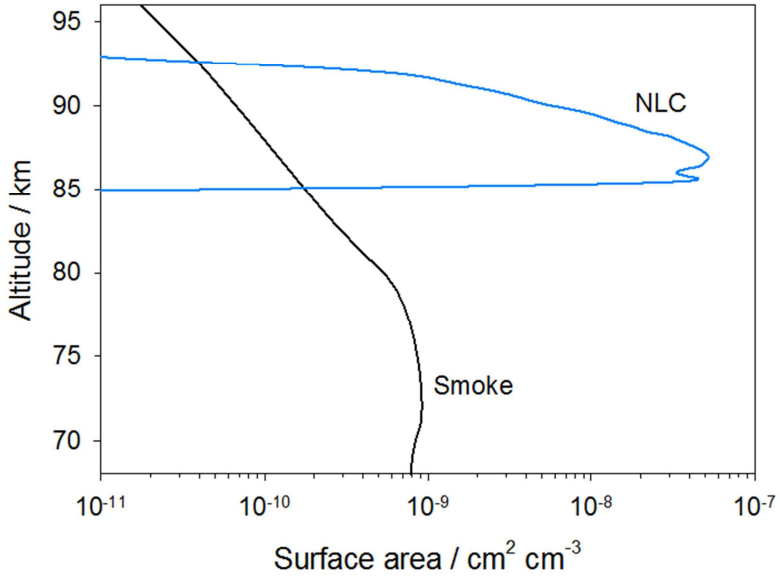

411

412 **Figure 5**. Comparison of available surface area from MSPs measured by a rocket-
413 borne dust detector (Plane et al., 2014), and lidar measurements of a strong PMC
414 (Plane et al., 2004).

415

416 In fact, Hervig et al. (2012) used observations from the Solar Occultation For Ice
417 Experiment (SOFIE) spectrometer on the AIM satellite to deduce that PMC particles
418 contain between 0.01 and 3% by volume of meteoric smoke. This implies that if an
419 ice particle had a typical radius of 50 nm, then the residual MSP particle left after
420 sublimation would have a radius of between 2.4 and 15.8 nm (assuming a density of
421 2 g cm^{-3}). This can be compared to the predictions of a 1-D microphysical model
422 where MSP growth occurs by coagulation, and the global input of ablated cosmic
423 dust is 5 t d^{-1} (Plane et al., 2014): the concentration of particles larger than 2 nm is
424 64 cm^{-3}, and larger than 15 nm is only 0.2 cm^{-3}. Since the typical concentration of
425 PMC ice particles in a strong cloud is 200 cm^{-3} (Plane et al., 2004), this would

represent a dramatic ice-catalyzed coagulation if the PMC particles contained meteoric smoke close to 3% by volume.

It is worth considering what conditions would be required to build up these MSP-enriched ice particles. We have recently shown by modelling the different cometary and asteroidal sources of cosmic dust entering the Earth's atmosphere that the ablation input is around 8 t d^{-1} (Carrillo-Sánchez et al., 2016). If a strong PMC was 1 km thick with a 200 cm^{-3} concentration of 50 nm ice particles (corresponding to the cloud in Figure 5 (Plane et al., 2004)), then it would take ~1.4 days of ablation input to build up a 0.01% volume of meteoric material in the ice, *if* all the ablated vapours directly entered the ice particles, and so is a lower limit to the time required. In fact, the average lifetime of individual ice particles in a strong PMC appears to be only around 5 hours (Kiliani et al., 2013), which implies that the same meteoric material would build up through several cycles of ice particle nucleation, growth and sublimation. This is possible because the Stokes settling velocity of a "typical" MSP with a radius of 2 nm and a density of 2 g cm^{-3} is on the order of 10^{-3} m s^{-1} at 1 Pa, which is much smaller than the vertical wind during polar summer (Plane et al., 2015). Thus, the net motion of these MSPs can be upward during PMC season, back into a region where nucleation could occur. Note that in order to build up 3% by volume of smoke in the ice particles (the upper end of the range deduced from satellite observations (Hervig et al., 2012)), would take 407 days which is more difficult to explain.

6. Summary and conclusions

In this study we have used experiments on ice films within a UHV chamber to investigate the binding and reactivity of Mg and K on ice at temperatures of 110 – 140 K. Both metals were readily adsorbed under these conditions but were found not to co-desorb with the ice layer upon sublimation. Experimental sputtering showed that the metals are left as residuals after the ice sublimes, suggesting that in the case of PMC ice particles, or icy particles in space, the metals would remain in the solid phase after ice sublimation. We hypothesise that the depletion of metal during a PMC event would lead to the formation of a population of large (≥ 2 nm radius) MSPs after the cloud sublimated. The effects on the mesosphere of this process require future modelling to account for cloud microphysics and competing MSP formation mechanisms. Energetic sputtering by 500 eV Ar^+ and Kr^+ of metal dosed ice layers also showed that Mg was unreactive, while K formed KOH on the ice surface. These observations were supported by electronic structure calculations, with an Mg atom shown to be unreactive and only binding at an irregularity in the ice structure, while an initially adsorbed K atom requires relatively little energy to insert into a surface H_2O to produce KOH and a dangling H atom. The calculations also explain a previous observation that adsorbed Fe reacts on low-temperature ice to produce $Fe(OH)_2$.

Acknowledgements

TPM thanks the Natural Environment Research Council (NERC) for a PhD studentship. VLF and JMCP were supported by the European Research Council (project number 291332 – CODITA). BJM was supported by the European Research Council (project numbers: 648661 - MarineIce and 240449 - ICE).

References

Baumgarten, G., Fiedler, J., Lübken, F.J., von Cossart, G., 2008. Particle properties and water content of noctilucent clouds and their interannual variation. J. Geophys. Res. 113, D06203.

Brown, D.E., George, S.M., Huang, C., Wong, E.K.L., Rider, K.B., Smith, R.S., Kay, B.D., 1996. H_2O condensation coefficient and refractive index for vapor-deposited ice from molecular beam and optical interference measurements. J. Phys. Chem. 100, 4988-4995.

Campins, H., Hargrove, K., Pinilla-Alonso, N., Howell, E.S., Kelley, M.S., Licandro, J., Mothé-Diniz, T., Fernández, Y., Ziffer, J., 2010. Water ice and organics on the surface of the asteroid 24 Themis. Nature 464, 1320-1321.

Carrillo-Sánchez, J.D., Nesvorný, D., Pokorný, P., Janches, D., Plane, J.M.C., 2016. Sources of cosmic dust in the Earth's atmosphere. Geophys. Res. Lett. 43, 11979-11986.

Ciesla, F.J., Cuzzi, J.N., 2006. The evolution of the water distribution in a viscous protoplanetary disk. Icarus 181, 178-204.

Cuzzi, J.N., Zahnle, K.J., 2004. Material Enhancement in Protoplanetary Nebulae by Particle Drift through Evaporation Fronts. Astrophys. J. 614, 490.

494 Dawkins, E.C.M., Plane, J.M.C., Chipperfield, M.P., Feng, W., 2015. The near-global
495 mesospheric potassium layer: Observations and modeling. J. Geophys. Res. 120,
496 7975-7987.

497 Driss, T., Vishnu, R., Juan, A.S., Michael, K.S., Joshua, P.E., 2017. Detection of
498 Water and/or Hydroxyl on Asteroid (16) Psyche. Astrophys. J. 153, 31.

499 Dzyurkevich, N., Turner, N.J., Henning, T., Kley, W., 2013. Magnetized Accretion
500 and Dead Zones in Protostellar Disks. Astrophys. J. 765, 114.

501 Fiedler, J., Baumgarten, G., von Cossart, G., 2003. Noctilucent clouds above
502 ALOMAR between 1997 and 2001: Occurrence and properties. J. Geophys. Res.
503 108, 8453.

504 Filacchione, G., De Sanctis, M.C., Capaccioni, F., Raponi, A., Tosi, F., et al., 2016.
505 Exposed water ice on the nucleus of comet 67P/Churyumov–Gerasimenko. Nature
506 529, 368-372.

507 Foresman, J.B., Frisch, A., 1996. Exploring chemistry with electronic structure
508 methods. Gaussian, Inc.

509 Frankland, V.L., Plane, J.M.C., 2015. Fe embedded in ice: the impacts of sublimation
510 and energetic particle bombardment. J. Atmos. Solar-Terr. Phys. 127, 103-110.

511 Fraser, H.J., Collings, M.P., McCoustra, M.R.S., Williams, D.A., 2001. Thermal
512 desorption of water ice in the interstellar medium. Mon. Not. Roy. Astron. Soc. 327,
513 1165-1172.

514 Frisch, M.J., Trucks, G.W., Schlegel, H.B., Scuseria, G.E., Robb, M.A., et al., 2009.
515 Gaussian 09. Gaussian, Inc.

516 Gadsden, M., 1982. Noctilucent clouds. Space Sci. Rev. 33, 279-334.

517 Galvez, O., Mate, B., Herrero, V.J., Escribano, R., 2008. Trapping and adsorption of
518 CO2 in amorphous ice: A FTIR study. Icarus 197, 599-605.

519 Gardner, C.S., Plane, J.M.C., Pan, W.L., Vondrak, T., Murray, B.J., Chu, X.Z., 2005.
520 Seasonal variations of the Na and Fe layers at the South Pole and their implications
521 for the chemistry and general circulation of the polar mesosphere. J. Geophys. Res.
522 110, D1030210.

523 Hervig, M.E., Deaver, L.E., Bardeen, C.G., Russell, J.M., III, Bailey, S.M., Gordley,
524 L.L., 2012. The content and composition of meteoric smoke in mesospheric ice
525 particles from SOFIE observations. J. Atmos. Solar-Terr. Phys. 84-85, 1-6.

526 Hervig, M.E., Thompson, R.E., McHugh, M., Gordley, L.L., Russell, J.M., Summers,
527 M.E., 2001. First confirmation that water ice is the primary component of polar
528 mesospheric clouds. Geophys. Res. Lett. 28, 971-974.

529 Kiliani, J., Baumgarten, G., Lübken, F.J., Berger, U., Hoffmann, P., 2013. Temporal
530 and spatial characteristics of the formation of strong noctilucent clouds. J. Atmos.
531 Solar-Terr. Phys. 104, 151-166.

532 Langowski, M.P., von Savigny, C., Burrows, J.P., Feng, W., Plane, J.M.C., et al.,
533 2015. Global investigation of the Mg atom and ion layers using SCIAMACHY/Envisat
534 observations between 70 and 150 km altitude and WACCM-Mg model results.
535 Atmos. Chem. Phys. 15, 273-295.

536 Lewis, J.S., 2004. Physics and chemistry of the solar system. Elsevier Academic
537 Press.

538 Lübken, F.-J., Höffner, J., 2004. Experimental evidence for ice particle interaction
539 with metal atoms at the high latitude summer mesopause region. Geophys. Res.
540 Lett. 31, L08103.

541 Malkin, T.L., Murray, B.J., Salzmann, C.G., Molinero, V., Pickering, S.J., Whale, T.F.,
542 2015. Stacking disorder in ice I. Phys. Chem. Chem. Phys. 17, 60-76.

543 Mangan, T.P., Frankland, V.L., Plane, J.M.C., 2015. CO_2 trapping in amorphous H_2O
544 ice: Relevance to polar mesospheric cloud particles. J. Atmos. Solar-Terr. Phys. 127,
545 92-96.

546 Murray, B.J., Malkin, T.L., Salzmann, C.G., 2015. The crystal structure of ice under
547 mesospheric conditions. J. Atmos. Solar-Terr. Phys. 127, 78-82.

548 Murray, B.J., Plane, J.M.C., 2005. Uptake of Fe, Na and K atoms on low-
549 temperature ice: implications for metal atom scavenging in the vicinity of polar
550 mesospheric clouds. Phys. Chem. Chem. Phys. 7, 3970-3979.

551 Patashnick, H., Rupprecht, G., 1975. The size dependence of sublimation rates for
552 interplanetary ice particles. Astrophys. J. 197, 79-82.

553 Plane, J.M.C., 2003. Atmospheric Chemistry of Meteoric Metals. Chem. Rev. 103,
554 4963-4984.

555 Plane, J.M.C., Feng, W., Dawkins, E.C.M., 2015. The Mesosphere and Metals:
556 Chemistry and Changes. Chem. Rev. 115, 4497-4541.

557 Plane, J.M.C., Murray, B.J., Chu, X.Z., Gardner, C.S., 2004. Removal of meteoric
558 iron on polar mesospheric clouds. Science 304, 426-428.

559 Plane, J.M.C., Saunders, R.W., Hedin, J., Stegman, J., Khaplanov, M., et al., 2014.
560 A combined rocket-borne and ground-based study of the sodium layer and charged
561 dust in the upper mesosphere. J. Atmos. Solar-Terr. Phys. 118, 151-160.

562 Podolak, M., Zucker, S., 2004. A note on the snow line in protostellar accretion disks.
563 Meteorit. Planet. Sci. 39, 1859-1868.

564 Pollack, J.B., Hollenbach, D., Beckwith, S., Simonelli, D.P., Roush, T., Fong, W.,
565 1994. Composition and radiative properties of grains in molecular clouds and
566 accretion disks. Astrophys. J. 421, 615-639.

567 Pont, F., 2014. Alien skies: planetary atmospheres from Earth to exoplanets.
568 Springer.

569 Raizada, S., Rapp, M., Lübken, F.J., Höffner, J., Zecha, M., Plane, J.M.C., 2007.
570 Effect of ice particles on the mesospheric potassium layer at Spitsbergen (78°N). J.
571 Geophys. Res. 112, D08307.

572 Rapp, M., Lubken, F.J., 2004. Polar mesosphere summer echoes (PMSE): review of
573 observations and current understanding. Atmos. Chem. Phys. 4, 2601-2633.

574 Sack, N.J., Baragiola, R.A., 1993. Sublimation of vapor-deposited water ice below
575 170 K, and its dependence on growth conditions. Phys. Rev. B 48, 9973-9978.

576 Safarik, D.J., Mullins, C.B., 2004. The nucleation rate of crystalline ice in amorphous
577 solid water. J. Chem. Phys. 121, 6003-6010.

578 Sato, T., Okuzumi, S., Ida, S., 2016. On the water delivery to terrestrial embryos by
579 ice pebble accretion. Astron. Astrophys. 589, A15.

580 Saunders, R.W., Mohler, O., Schnaiter, M., Benz, S., Wagner, R., et al., 2010. An
581 aerosol chamber investigation of the heterogeneous ice nucleating potential of
582 refractory nanoparticles. Atmos. Chem. Phys. 10, 1227-1247.

583 Saunders, R.W., Plane, J.M.C., 2006. A laboratory study of meteor smoke
584 analogues: Composition, optical properties and growth kinetics. J. Atmos. Solar-Terr.
585 Phys. 68, 2182-2202.

586 Thomas, G.E., 1991. Mesospheric clouds and the physics of the mesopause region.
587 Rev. Geophys. 29, 553-575.

588 Viehl, T.P., Hoeffner, J., Luebken, F.J., Plane, J.M.C., Kaifler, B., Morris, R.J., 2015.
589 Summer time Fe depletion in the Antarctic mesopause region. J. Atmos. Solar-Terr.
590 Phys. 127, 97-102.

591 von Cossart, G., Fiedler, J., von Zahn, U., 1999. Size distributions of NLC particles
592 as determined from 3-color observations of NLC by ground-based lidar. Geophys.
593 Res. Lett. 26, 1513-1516.

594 Vondrak, T., Meech, S.R., Plane, J.M.C., 2009. Photoelectric emission from the
595 alkali metal doped vacuum-ice interface. J. Chem. Phys. 130, 054702.

596 Vondrak, T., Plane, J.M.C., Meech, S.R., 2006. Influence of submonolayer sodium
597 adsorption on the photoemission of the Cu(111)/water ice surface. J. Chem. Phys.
598 125, 224702.

599 Yakshinskiy, B.V., Madey, T.E., 2001. Electron- and photon-stimulated desorption of
600 K from ice surfaces. J. Geophys. Res. 106, 33303-33307.

601

Highlights

- Mg and K species deposited on ice do not co-desorb when the ice sublimes
- Mg is unreactive on ice surface, while K reacts to form KOH
- An effective and distinct MSP coagulation mechanism occurring in PMCs is proposed